Improving Crystallization Behaviors of Isotactic Polypropylene via a New POSS-Sorbitol Compound

Baixuan Feng,[1] Zhenguang Li,[1] Guanyun Chen,[1] Kongying Zhu,[2] Yunhui Zhao,[1] Xiaoyan Yuan[1]
[1] *School of Materials Science and Engineering, and Tianjin Key Laboratory of Composite and Functional Materials, Tianjin University, Tianjin 300072, China*
[2] *Analysis and Measurement Center, Tianjin University, Tianjin 300072, China*

A new compound was synthesized by chemical combination of (3-mercapto)propyl-heptaisobutyl polyhedral oligomeric silsesquioxane (POSS-SH) and 1,3:2,4-bis(3,4-dimethylbenzylidene) sorbitol (DMDBS) via epichlorohydrin while hydroxyl groups were still retained in the product POSS-DMDBS. The prepared POSS-DMDBS was introduced into isotactic polypropylene (iPP) to improve crystallization behaviors of iPP and obtain nanocomposites with suitable mechanical properties. Crystallization and mechanical properties of iPP/POSS-DMDBS were systematically investigated by wide-angle X-ray diffraction, polarization microscopy, atomic force microscopy, differential scanning calorimetry, and tensile tests. The spherulite size of the modified iPP was obviously decreased with the addition of POSS-DMDBS, while the crystallization temperature was increased by 5°C to 9°C depending on the content of POSS-DMDBS incorporated. POSS-DMDBS exhibited relatively higher nucleating efficiency on iPP which is similar to that of DMDBS, confirmed by the increased crystallization temperature. It was also found that the tensile modulus of iPP after adding POSS-DMDBS increased significantly with respect to pristine iPP, but the elongation values decreased. Introduction of POSS-DMDBS in content less than 1 wt% could bring about effective influence on the crystallization behaviors of iPP, demonstrating its potential applications. POLYM. ENG. SCI., 57:357–364, 2017. © 2016 Society of Plastics Engineers

INTRODUCTION

As a kind of hybrid organic–inorganic compounds, polyhedral oligomeric silsesquioxanes (POSS) received dramatic attention in recent years for development of polymer nanocomposites [1–3]. Different from other inorganic modifiers, POSS has a special cage structure and eight organic groups, which provide it with special functionalities, such as oxidation resistance, thermal stability, and compatibility with various host polymers [4]. According to above mentioned features, POSS can be introduced into various polymers by blending, crosslinking, grafting, or copolymerization [5–7].

Incorporating POSS into polypropylene matrix and the effect on the composite properties have been investigated [8]. Notably, in most reports, the amount of POSS added in isotactic polypropylene (iPP) was higher than 1 wt% [9], which may limit the industrial applications for the stiff price of POSS. Conversely, the crystallization properties of iPP could not be improved by POSS sufficiently. Fina et al. reported that octamethyl-POSS could act as a nucleating agent to increase the crystallization temperature of iPP by 2–3°C depending on the POSS content, whereas octaisobutyl-POSS and octaisooctyl-POSS conversely decreased the crystallization temperature of iPP [1]. As a semicrystalline polymer, the crystallite structure of iPP has been studied intensively owing to the significant effect on processability, transparency, and mechanical properties [10, 11]. For this purpose, nucleating agents are used to enhance the crystallization rate and thus shorten the cycle time in manufacturing processes. By using a suitable nucleating agent, the spherulite size could also be decreased, so that the optical clarity and mechanical properties of the product can be improved [12, 13].

Sorbitol derivatives have been widely used as nucleating and clarifying agents commercially with high nucleating efficiency and relatively low cost [14]. The specially molecular structure of 1,3:2,4-di(3,4-dimethylbenzylidene) sorbitol (DMDBS) made it able to self-assemble in the iPP melt and form fibrillar network [15–17], that can increase nucleating efficiency and decrease spherulite size. DMDBS has a butterfly shaped molecule structure with hydrophobic "wings" and hydrophilic "body" [18]. The phenyl rings with two methyl groups enable DMDBS to dissolve in the iPP melt, while the two hydroxyl groups in "body" formed hydrogen bond between DMDBS molecules. The hydrogen bonding, however, plays a major role in the formation of network along with the π–π interactions between the phenyl groups of the same chirality for network formation [4, 19].

The interactional mechanism between hydroxylated POSS (POSS-OH) and DMDBS in iPP melt via hydrogen bonds has been studied [19]. Roy et al. prepared melt spun monofilament fibers of iPP with the addition of di(benzylidene)-sorbitol (DBS) and POSS containing phenyl side-chain and silanol functionalities, and the obtained compound exhibited significantly improved mechanical properties [4, 19, 20]. Up to now, few papers have reported the effect of compounds combining POSS and DMDBS with chemical bonding on the properties of iPP. Our previous publication investigated chemically combined use of (3-mercapto)propyl-heptaisobutyl POSS (POSS-SH) and DMDBS, and the subsequent impact on modified iPP properties [21]. However, the hydroxyl groups were not preserved in the DMDBS structure, which may inhibit the formation of the fibrillar network via hydrogen bonding.

To retain hydroxyl groups in the combined POSS-DMDBS compound, in the present research, chemical reaction of POSS-SH with DMDBS was carried out by epichlorohydrin (ECH). The objective of this study was to investigate the crystallization behaviors of the modified iPP by the prepared nucleating agent POSS-DMDBS in comparison with DMDBS as well as the blend of DMDBS and POSS-SH (POSS/DMDBS). Analyses of

Correspondence to: K. Zhu; e-mail: ausky@tju.edu.cn
DOI 10.1002/pen.24430
Published online in Wiley Online Library (wileyonlinelibrary.com).

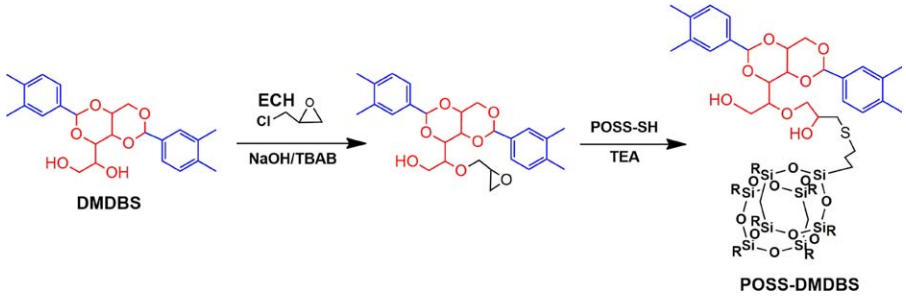

FIG. 1. Synthesis of POSS-DMDBS from POSS-SH and DMDBS via epichlorohydrin. The obtained POSS-DMDBS compound still has hydroxyl groups in its structure for network formation when melted with iPP. [Color figure can be viewed at wileyonlinelibrary.com.]

differential scanning calorimetry (DSC), polarized optical microscopy (POM), atomic force microscopy (AFM), and tensile tests were performed to examine the effect of the additives on crystallization behaviors and mechanical properties of iPP.

EXPERIMENTAL

Materials

iPP (K1008) was obtained in the form of pellets from Yanshan Petrochemical Co., Ltd. (Beijing, China) with melt flow index 10 g/10 min (ASTM D1238), density 0.905 g/cm^3, and melting temperature (T_m) 162°C. This grade of iPP was ensured not contain any nucleating agent according the information obtained from the supplier.

POSS-SH was obtained in the form of a white powder from Hybrid Plastics (Hattiesburg, MS) with molecular weight 891.63 g/mol and T_m of 352°C. DMDBS was obtained in the form of a white powder from Zhichu Co., Ltd. (Yantai, China) with molecular weight 414.49 g/mol and T_m of 275°C. Epichlorohydrin (ECH) and tetrabutylammonium bromide (TBAB) were obtained from J&K Chemical Technology Co., Ltd. (Beijing, China). Catalyst and reactive solvents including triethylamine (TEA), *N*,*N*-dimethylformamide (DMF) and tetrahydrofuran (THF) were supplied by Kemiou Chemical Reagent Co., Ltd (Tianjin, China). All of the above materials were used without further treatment.

Synthesis of POSS-DMDBS

POSS-DMDBS was prepared according to the following procedures. First, 0.5 g DMDBS was fully dissolved in 25 mL DMF in a 50-mL three-necked flask under 70°C, and then 0.14 g NaOH and 0.023 g TBAB were added. After rigorous stirring for 5 min, 0.5 mL ECH was added in 40 min by injection pump and the system was kept at 60°C for 8 h. After filtration and washing with water for five times to remove the residual NaOH, DMF, and TBAB, the resultant was dried for 24 h to obtain DMDBS-ECH as intermediate product. Second, 0.5 g DMDBS-ECH and 0.83 g POSS-SH were dissolved in the mixed solvent of 25 mL DMF and 25 mL THF. Then 0.15 mL TEA was added and the reaction lasted for at least 24 h. After rotary evaporation and filtration to remove THF and POSS-SH, the resultant was purified under distillation and dried for 24 h to obtain POSS-DMDBS. The chemical structures of DMDBS, POSS-SH and the synthesis route of POSS-DMDBS are shown in Fig. 1.

Preparation of iPP Samples

DMDBS, POSS-SH, POSS-DMDBS, and POSS/DMDBS was introduced into iPP individually by melt-mixing in an internal mixer (XSS-300, China), and the samples were designated as iPP/DMDBS, iPP/POSS, iPP/POSS-DMDBS, and iPP/POSS/DMDBS, respectively. A certain amount of antioxidant was added during the melt mixing. The compositions of the samples are shown in Table 1. Among the compositions, POSS-DMDBS was charged at a content of 0.3, 0.6, and 1 wt%, which were recorded as iPP/POSS-DMDBS1, iPP/POSS-DMDBS2, and iPP/POSS-DMDBS3, respectively. The amount of substance of POSS-DMDBS in POSS-DMDBS3 is approximately equal to DMDBS and POSS-SH in the corresponding samples. First, iPP was heated to melt in the mixer at 180°C and then blended powder mixtures were put into the mixing chamber. The compounds were mixed for 5 min at 180°C with the screw rotation rate of 32 rpm. The samples were molded by compressing in a homemade stainless steel frame (140 mm × 140 mm × 2 mm) at 220°C for further experiments and analysis.

Characterizations

^{1}H-Nuclear Magnetic Resonance. ^{1}H-nuclear magnetic resonance (^{1}H NMR) experiments were recorded at 11.75T with a Varian Inova 500 MHz NMR spectrometer at 25°C. Dimethyl sulfoxide-d6 (DMSO-d6) was used as solvent, and the chemical shifts were referenced to tetramethylsilane at 0 ppm.

Wide-Angle X-ray Diffraction. Analysis of wide-angle X-ray diffraction (WAXD) was performed on a D8 Advance X-ray diffractometer (Bruker, Germany). A monochromatic X-ray radiation with a wavelength (λ) of 1.54 Å (Cu Kα) was used with diffraction angle $2\theta = 5$–$45°$ and scanning speed of 2° min^{-1}. Identification was based on a reflected X-ray peak intensity analysis at a defined 2θ angle.

Polarized Optical Microscopy. The formation of spherulites of the compounds was examined by POM. An Axioskop 40 Pol (Carl Zeiss, Germany) optical microscope equipped with a MicroPublisher 3.3 RTV CCD was used in cross-polarized mode. Samples were heated to 220°C and kept for 5 min between two glass slides on a hot stage to melt the residual crystals. At this time the polymer films of thickness around about 100 μm were prepared by compressing the melt, subsequently the samples were cooled down to 140°C at a cooling

DOI 10.1002/pen

TABLE 1. Data obtained from DSC non-isothermal crystallization exothermic peaks and tensile mechanical properties of samples.

	Characteristic data from DSC									Tensile properties		
Sample[a]	T_{onset} (°C)	T_{onset}-T_E (°C)	n	Z_c ($s^{-n}\times10^{-4}$)	Z_t ($s^{-n}\times10^{-4}$)	$t_{1/2}$ (s)	T_c (°C)	NE (%)	X_c (%)	Young's modulus (MPa)	Tensile strength (MPa)	Elongation at break (%)
iPP	122.8	10.6	2.37	53.3	1.94	31.3	116.0	0	55.4	830.4 ± 54.9	34.09 ± 3.94	608 ± 168
iPP/DMDBS	134.3	9.6	2.37	773.8	3.03	25.9	130.2	59.2	59.5	1,021.6 ± 35.8	36.21 ± 1.27	510.4 ± 0.77
iPP/POSS	122.9	11.9	2.35	48.6	1.91	32.9	117.8	7.5	55.9	846.0 ± 20.9	31.04 ± 1.10	512.9 ± 1.48
iPP/POSS/DMDBS	133.2	12.5	2.30	136.8	2.27	32.5	128.5	52.1	58.9	967.0 ± 40.3	34.62 ± 0.73	511.2 ± 0.84
iPP/POSS–DMDBS1	132.2	17.1	2.30	0.06	0.63	57.1	122.0	25.0	57.1	965.7 ± 31.0	34.54 ± 1.58	499.4 ± 0.69
iPP/POSS–DMDBS2	132.6	16.6	2.23	2.99	1.20	48.3	122.8	28.3	57.6	971.6 ± 48.0	34.59 ± 1.29	499.9 ± 1.24
iPP/POSS–DMDBS3	130.9	12.0	2.29	244.1	2.50	31.8	126.1	42.1	60.4	987.6 ± 44.0	34.37 ± 1.12	489.7 ± 1.43

[a]Samples iPP/POSS–DMDBS1, iPP/POSS–DMDBS2 and iPP/POSS–DMDBS3 contain 0.3, 0.6 and 1 wt% of POSS–DMDBS, respectively.

rate of −30°C/min and the crystallization behavior of the samples were determined under isothermal condition.

Atomic Force Microscopy. AFM observation was performed with a CSPM5500A of Being Nano-Instruments Ltd., Guangzhou, China, equipped with E-type vertical engage piezoelectric scanner. The phase and height images were obtained simultaneously while the instrument was operated in the tapping mode. Samples were prepared by compression molding and their surface was etched with 30 mL permanganate solution for 1 h [22].

Differential Scanning Calorimetry. Thermal properties such as enthalpies and crystallization temperature (T_c) were tested under nitrogen gas atmosphere using a Netzsch 204 F1 differential scanning calorimetry (DSC, Germany). The melt-mixed iPP samples were heated at a rate of 10°C/min from 50°C to 220°C. Then the melt was kept at 220°C for 5 min to erase the heating history before the recrystallization process with the materials cooled from 220°C to 50°C at a rate of −10°C/min. T_c was determined as the crystallization peak temperature of cooling scans and the crystallinity (X_c) of the samples was determined from the melting fusion enthalpy (ΔH_m) by *Eq. 1*. ΔH_0 is the enthalpy of crystallization of 100% crystalline iPP ($\Delta H_0 = 177$ J/g) [22].

$$X_c(\%) = \Delta H_m / \Delta H_0 \times 100\% \quad (1)$$

The nucleation efficiency (NE) can be represented by the *Eq. 2* [23].

$$\mathrm{NE} = 100(T_c - T_{c1})/(T_{c2max} - T_{c1}) \quad (2)$$

where, T_c and T_{c1} are the crystallization temperatures of the polymer nucleated and non-nucleated with nucleating agent, respectively. The value of T_{c2max} was referred to the highest achievable peak temperature at 140°C, which was obtained from the self-nucleation experiments [24].

The Avrami equation [25] has been expressed as follows:

$$1 - X_t = \exp(-Z_t t^n) \quad (3)$$

where, n is the Avrami exponent, Z_t is the Avrami rate constant and X_t is the relative crystallinity at time t, defined by the *Eq. 4*.

$$X_t = \frac{X_t(t)}{X_t(\infty)} = \frac{\int_0^t (dH(t)/dt)dt}{\int_0^\infty (dH(t)/dt)dt} \quad (4)$$

where, $(dH(t)/dt)$ denotes the heat flow. $X_t(t)$ and $X_t(\infty)$ represent the absolute crystallinity at time t and at the termination of the crystallization process, respectively [26]. Taking a double logarithm of the *Eq. 5* gives:

$$\ln[-\ln(1 - X_t)] = \ln Z_t + n \ln t \quad (5)$$

The Avrami equation shows the relation of X_t and time (t), therefore temperature should be converted to time. Therefore, the Avrami exponent n and the crystallization rate parameter Z_t could be estimated from the slope and intercept of the straight-line portion in the plot of $\ln[-\ln(1 - X_t)]$ versus $\ln t$ for the crystallization process of iPP.

Considering the non-isothermal nature of the crystallization process, Jeziorny pointed out that the Avrami rate constant Z_t should be corrected by introducing the cooling rate D. The final form of the crystallization rate parameter at non-isothermal condition is shown:

$$\ln Z_c = \frac{\ln Z_t}{D} \quad (6)$$

According to the literature [26], it could be calculated that the half crystallization time $t_{1/2}$ by applying the *Eq. 7*.

$$t_{1/2} = \left(\frac{\ln 2}{Z_t}\right)^{1/n} \quad (7)$$

Tensile Properties. The tensile measurements were carried out according to international standard ISO 527-1 by using a universal testing machine (Testometric M350-20KN, UK) with a 2500N loadcell. The values of tensile modulus, tensile strength, and elongation at break were determined. The tensile tests were performed at 20 mm/min with 20 mm in gauge length. The reported values of the tensile properties were average of five independent measurements for each specimen.

RESULTS AND DISCUSSION

Synthesis of POSS-DMDBS

The ^{1}H-NMR spectra of DMDBS, POSS-SH, and POSS-DMDBS samples are shown in Fig. 2. The typical spectra of δ_H

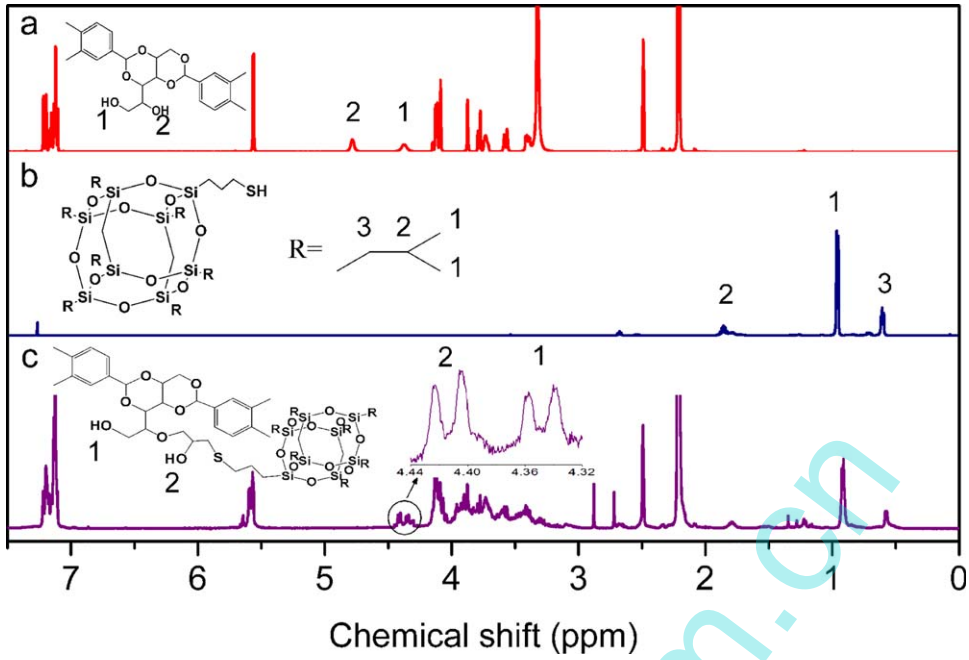

FIG. 2. [1]H-NMR spectra of (a) DMDBS, (b) POSS-SH, and (c) POSS-DMDBS. [Color figure can be viewed at wileyonlinelibrary.com.]

in DMDBS (Fig. 2a) at 4.4 and 4.8 ppm were attributed to the two types of hydroxyl groups. The signals of δ_H at 2.6, 2.7, and 2.9 ppm were the contribution of isobutyl group in polysilsesquioxane (Fig. 2b). The characteristic peaks of isobutyl group of polysilsesquioxane at 2.6, 2.7, and 2.9 ppm, as well as the characteristic peaks of hydroxyl groups at 4.34 and 4.42 ppm in Fig. 2c indicated that POSS-DMDBS was synthesized and the hydroxyl groups in DMDBS were retained successfully.

Crystallization

Figure 3 presents WAXD diffractograms of iPP, iPP/DMDBS, iPP/POSS, iPP/POSS/DMDBS, and iPP/POSS-DMDBS samples. In all considered samples α-crystalline formation was detected. The characteristic reflections at angles of 2θ (14.2°, 17.0°, 18.8°, 21.2°, and 22.0°), corresponded to the crystalline planes (110), (040), (130), (111), and (041), respectively [19]. There is no obvious change in diffraction peak can be observed in the curves, it can be inferred that DMDBS, POSS, and POSS-DMDBS did not lead to changes in polymorph. Overall, α-crystalline predominates in crystallization structure of all iPP samples, therefore, only α-crystalline of iPP will be discussed in the next section.

As we known, nanofibrillar networks are formed as sorbitol crystallizing in the iPP melt. These nanofibrils act as heterogeneous nucleation sites for iPP crystallization that leads to formation of smaller size spherulites. The size of spherulites in the crystallization process of iPP could be observed by optical microscope.

Polarized light micrographs taken from samples crystallized isothermally at 140°C are presented in Fig. 4. The profile of spherulites of neat iPP could be clearly observed (Fig. 4a). Almost the radius of each spherulite is larger than 100 μm, and this phenomenon could be explained by the lower nucleation rate of neat iPP during the homogeneous nucleation process, which leads to lower nucleus density of neat iPP and renders larger room for each crystal nucleus growth. As the sufficient growing of iPP crystal nucleus, individual perfect spherulite with an obvious Maltese cross was observed, and the coarse branching radial structure and positive birefringence are discernible in the micrograph. The dimension of spherulites formed as iPP/POSS was in the same level of neat iPP.

DMDBS has higher nucleating efficiency for iPP, and the crystalline texture is evenly and individual spherulites cannot be distinguished in the polarized light micrographs. The size of spherulites in iPP containing DMDBS/POSS was similar to the size of iPP/DMDBS as seen in Fig. 4b and d. Although the

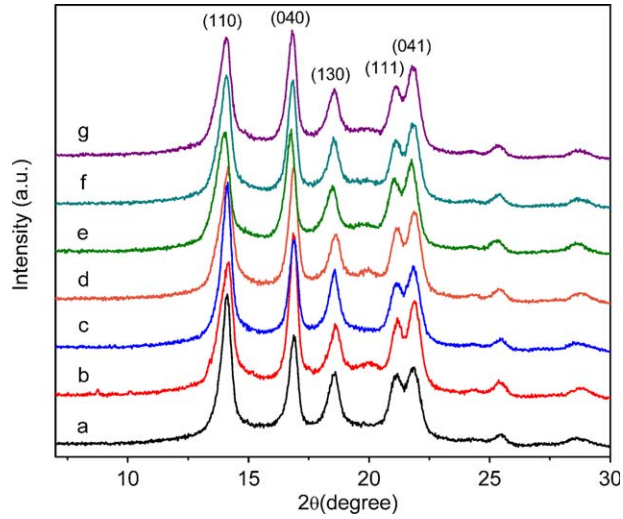

FIG. 3. WAXD diffraction patterns of (a) iPP, (b) iPP/DMDBS, (c) iPP/POSS, (d) iPP/DMDBS/POSS, (e) iPP/POSS-DMDBS1, (f) iPP/POSS-DMDBS2, and (g) iPP/POSS-DMDBS3. [Color figure can be viewed at wileyonlinelibrary.com.]

DOI 10.1002/pen

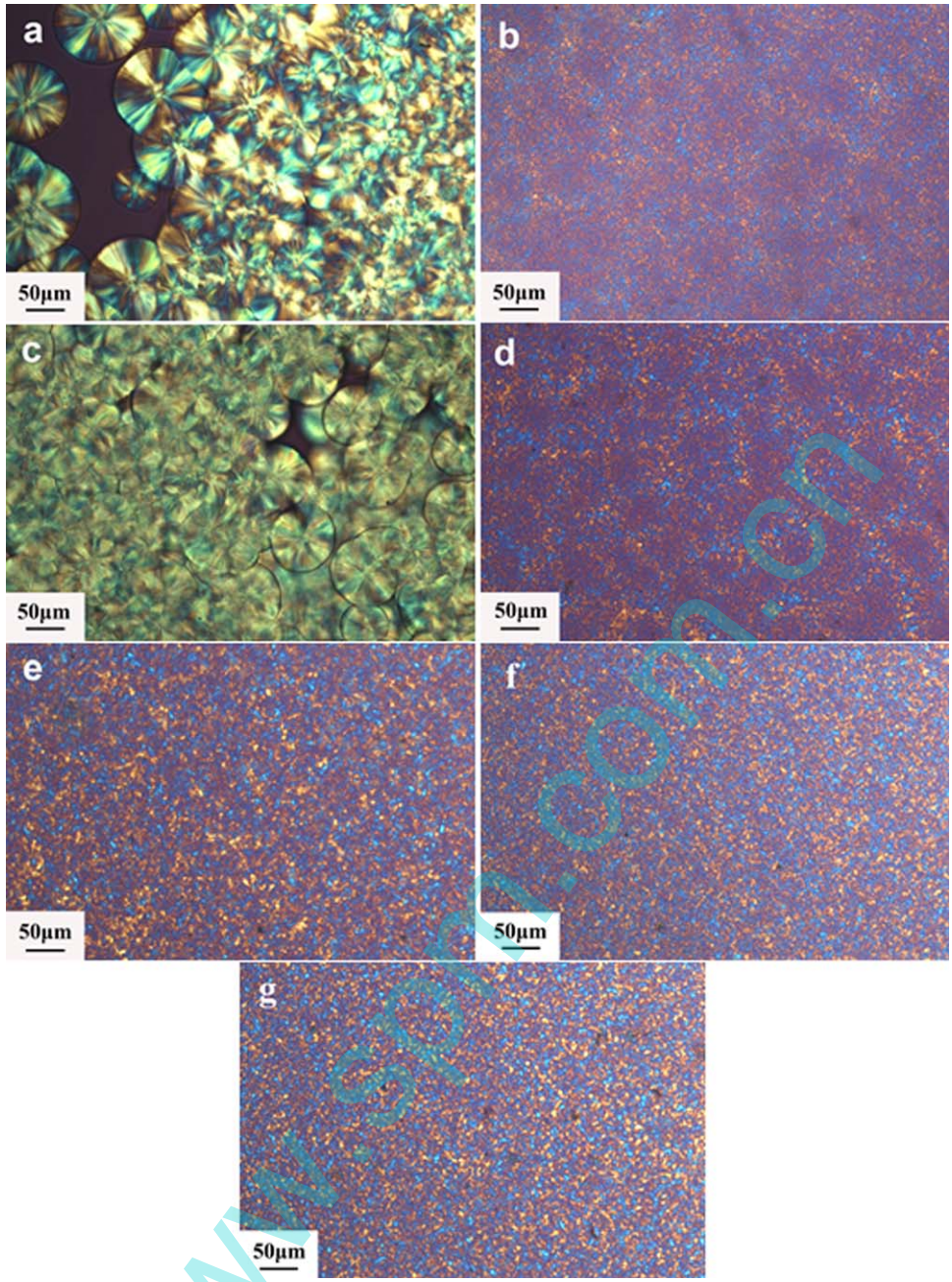

FIG. 4. Optical micrographs of spherulites of (a) iPP, (b) iPP/DMDBS, (c) iPP/POSS, (d) iPP/POSS/DMDBS, (e) iPP/POSS-DMDBS1, (f) iPP/POSS-DMDBS2 and (g) iPP/POSS-DMDBS3 upon cooling the melt from 220°C to 140°C at the rate of −20°C/min. [Color figure can be viewed at wileyonlinelibrary.com.]

formation of nanofibers was inhibited by POSS-SH by hydrogen bonding to some extent, DMDBS still act as efficient nucleating agent as observed in Fig. 4d.

The size of spherulites in the samples containing POSS-DMDBS (Fig. 4e–g) was found slightly larger than that in iPP/DMDBS/POSS. Aforementioned phenomenon elucidated that chemical bonding between DMDBS and POSS-SH has a greater inhibitive effect on the formation of nanofibril than hydrogen bonding, eventually leading to the decrease of nucleating efficiency.

Although the different spherulite sizes of modified iPP contained POSS-SH and other addictives are seen in the polarized micrographs, the spherulite outline of the iPP/DMDBS or iPP/POSS-DMDBS could not be observed clearly in polarized light micrographs, therefore we made a comparison of the crystalline structure in the AFM micrographs.

Figure 5 showed the formation of the spherulites in the samples containing DMDBS and POSS-DMDBS in the 3 × 3 μm AFM micrograph. The larger stiffness leads to a more positive phase shift and thus to a brighter contrast in the phase image [27]. Spherulites could be easily observed as bright spot because of its higher stiffness compared to that of the amorphous region in the phase image. Spherulites are homogenously dispersed and closely packed in iPP/DMDBS, and the grains have dimensions

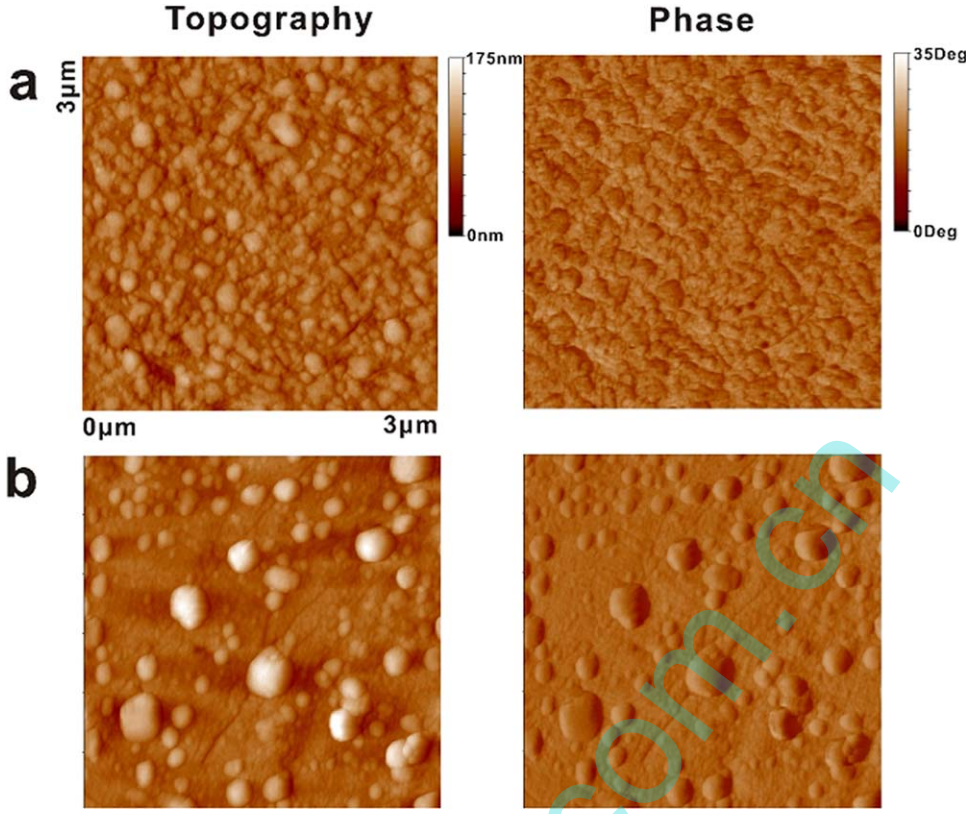

FIG. 5. AFM images showing the morphology of (a) iPP/DMDBS and (b) iPP/POSS-DMDBS3 after etched by permanganate solution for 1 h. [Color figure can be viewed at wileyonlinelibrary.com.]

between 50 nm and 150 nm as detected in Fig. 3a. The decreased spherulite size could be attributed to the import of DMDBS as discussed before in the optical properties.

Figure 5b shows 3 × 3 μm AFM height micrograph of the iPP sample containing POSS-DMDBS. iPP/POSS-DMDBS exhibits lower crystalline density compared to iPP/DMDBS, and large area of smooth surface around the spherulites can be seen in the image. The spherulites are distinguished into two sizes by the diameter of the grains. Some spherulites are in larger sizes with dimensions about 400 nm, and the others are in smaller sizes from 50 to 150 nm. This image exhibits a very different appearance compared with iPP/DMDBS, which could not be observed in polarized light micrographs. A conjectured explanation was that DMDBS can finely crystallize and self-assemble into nanofibrils to provide active nucleation sites. And then a huge amount of crystal nucleus born and grew closely in these sites until they contacted each other, eventually spherulite with very small sizes were formed due to the great crystalline density and limited space. In the POSS-DMDBS samples, the chemical bond between DMDBS and POSS restrained the formation of nanofibrils, so the density of the nucleus decreased. Space along the nanofibrils still got abundant active nucleations and small grains formed *in situ*, and the crystalline density greatly decreased in other space and caused the formation of larger grains.

Thermal Properties

From the perspective of technical application, it is important to study the thermal properties of polypropylene in non-isothermal crystallization process. DSC data were collected for various compositions (Fig. 6). Crystallization temperature defined as the peak of the crystallization exotherm curve, and represents the temperature where take the maximum of the heat flow. Compared with neat iPP, samples contained 0.3 wt% of DMDBS presented obvious increase in crystallization temperature. It is noteworthy that POSS-SH cannot act as heterogeneous nucleating agent in iPP/POSS efficiently, which presented crystallization temperature (117.8°C) and crystallinity (55.9%) similar to those of neat iPP (116.0°C and 55.4%). The addition of DMDBS and POSS-SH blend into iPP (iPP/POSS/DMDBS) effectively increased the crystallization temperature and crystallinity, which exhibited better nucleation effect than POSS-SH. However, the crystallization temperature of samples contain POSS/DMDBS was still lower than that of DMDBS, mainly attributing to the hydrogen-bonding between POSS-SH and DMDBS, which restrained the formation of the nanofibrils of DMDBS [21].

It could be seen in Table 1 that samples containing POSS-DMDBS (iPP/POSS-DMDBS1, iPP/POSS-DMDBS2, and iPP/POSS-DMDBS3) exhibit effective nucleation, and the crystallization temperature rises from 122.0°C to 126.1°C with the increase of POSS-DMDBS content from 0.3 wt% to 1 wt% in iPP. The crystallization temperatures of all these samples are lower than the sample of iPP/DMDBS and iPP/POSS/DMDBS, and this illustrated the chemical bonding between DMDBS and POSS further restrained the formation of the nanofibrils and receded the nucleation effect of DMDBS-POSS. The crystallinity also rises with the increase of POSS-DMDBS content in iPP,

DOI 10.1002/pen

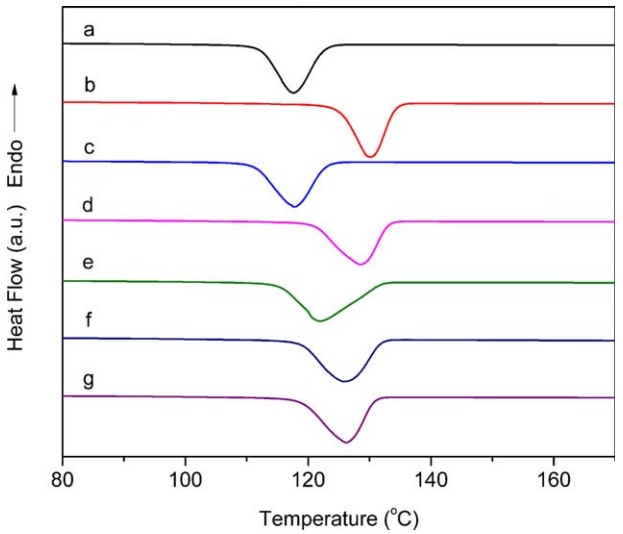

FIG. 6. DSC thermograms of (a) iPP, (b) iPP/DMDBS, (c) iPP/POSS, (d) iPP/POSS/DMDBS, (e) iPP/POSSDMDBS1, (f) iPP/POSS-DMDBS2, and (g) iPP/POSS-DMDBS3 at a cooling rate of −10°C/min after preheated at 220°C for 5 min. [Color figure can be viewed at wileyonlinelibrary.com.]

and the crystallinity of iPP/POSS-DMDBS3 (60.4%) is at the same level as that of iPP/DMDBS (59.5%).

Nucleation process has been studied to estimate the *NE* of the additives. The results reported in Table 1 show that with the increased concentration of POSS-DMDBS in the iPP matrix, the *NE* reached values from 25.0% to 42.1%. The iPP/POSS/DMDBS presented the higher *NE* of 52.1% for the same concentration of iPP/POSS-DMDBS (42.1%). Both POSS-DMDBS and DMDBS/POSS significantly raised the nucleation efficiency of POSS-SH (7.5%) and exhibited a little lower *NE* than that of DMDBS (59.2%). Nucleation efficiency (NE) depends on the nucleating effect of nucleating agent. Crystallization kinetics contains the relationship between crystallization behavior and crystallization conditions such as crystallization time and crystallization temperature, it is also influenced by the nucleating effect of nucleating agent.

The plot of $\ln[-\ln(1-X_t)]$ versus $\ln t$ according to the Avrami equation is shown in Fig. 7. It can be seen that the Avrami plot exhibited good linearity in a wide relative crystallinity range (1–98%), which indicates the Jeziorny mode is suitable for the non-isothermal crystallization kinetics of all the samples.

The Avrami exponent n, the rate constant Z_c and Z_t can be obtained from fitting the straight-line portion of Avrami plot and calculating the slop and intercept, $t_{1/2}$ can be obtained from *Eq. 7*, and all the values are listed in Table 1. It is shown from Table 1 that the Avrami exponent n of all samples is in a range of 2.2–2.4. The value of n depends on the crystallization mechanism, therefore, the additions of DMDBS, POSS-SH, POSS-DMDBS, and POSS/DMDBS can change neither the crystallization mechanism nor crystal growth geometries of iPP. It can be seen that the DMDBS involved iPP samples have the lower $t_{1/2}$ and higher Z_c than pure iPP, indicating the rapid crystallization rate of iPP/DMDBS. The $t_{1/2}$ of POSS related sample is slightly higher and the Z_c is lower than that of iPP, implying the nucleation rate and crystal growth is similar with iPP. In this aspect, POSS aggregate may form and attract iPP chains to attach POSS crystal surface and become a center of spherulite, which favors a large spherical crystal [28], therefore the sample iPP/POSS shows a little higher Z_c than pure iPP. When POSS and DMDBS were physical mixing in iPP, visible increase of Z_c is obtained compared with iPP/POSS and iPP, and indicated the sample contain both DMDBS and POSS have higher crystal growth. The Avrami rate constant Z_c of iPP/POSS-DMDBS with different POSS-DMDBS content is also listed in Table 1. With the increase of POSS-DMDBS content in iPP, the Z_c and $t_{1/2}$ changes from 0.63 to 2.5 and 57.1 to 31.8, respectively. When POSS-DMDBS was introduced in iPP at a relatively lower concentration, the nanofiber does not form completely and cannot act as a nucleating agent to increase the crystallization rate of iPP. With the increasing content of POSS-DMDBS was added, the formation of nanofiber can render more nucleation sites and accelerate the crystallization process of iPP. The Z_c of the iPP sample contained 1 wt% of POSS-DMDBS is higher, and $t_{1/2}$ is lower than that of iPP/POSS/DMDBS and iPP/POSS. It is indicated that POSS-DMDBS has a better effect on increasing the crystal growth rate than POSS/DMDBS and POSS at the same content, the residual hydroxyl may promote the formation of the fibrillar network and then increase the crystal growth.

Tensile Properties

The tensile properties of the samples are presented in Table 1. The samples PP/DMDBS offered 23% increase in tensile modulus compared to unfilled iPP, while iPP/POSS-DMDBS 3 and iPP/POSS/DMDBS offer about 19% and 16% increase in tensile modulus compared to the unfilled, respectively. The tensile properties shown in Table 1 present evident statistically difference according to the probability (p) values smaller than 0.05. The tensile modulus of iPP/POSS-DMDBS1, iPP/POSS-DMDBS2, and iPP/POSS-DMDBS3 also increased with the rise of POSS-DMDBS content from 0.3 to 1 wt%, this is attributing to the increasing nucleation density and crystallinity. However, tensile strength of the three samples was not improved in comparison with unfilled iPP, and decrease in elongation at break

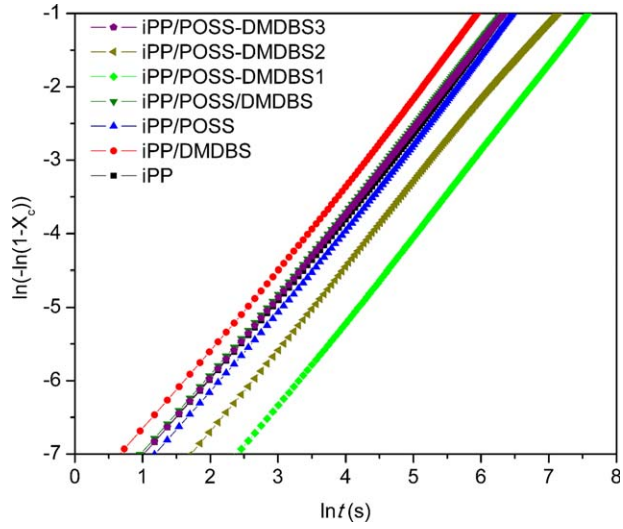

FIG. 7. Plots of $\ln[-\ln(1-X_c)]$ versus $\ln t$ for the samples. [Color figure can be viewed at wileyonlinelibrary.com.]

was also detected (Table 1). Therefore, it was assumed that the increase of nucleation density enhanced the strength and reduced the toughness of iPP. Both tensile modulus and tensile strength of iPP/POSS was lower than those of iPP/DMDBS, iPP/POSS/DMDBS and iPP/POSS-DMDBS, that could be attributed to the lower nucleation density and crystal growth rate, which caused by the interaction between POSS via mercapto groups according to the references 4.

CONCLUSIONS

Effects of chemically bonded DMDBS and POSS-SH, i.e., POSS-DMDBS on crystallization behaviors and mechanical properties of iPP were investigated. ^{1}H-NMR spectra demonstrated that POSS-SH was combined with DMDBS by covalent bond and hydroxyl groups were still remained in DMDBS-DMDBS molecules for keeping intermolecular hydrogen bonds. Similar to DMDBS or physical blend DMDBS/POSS, incorporation of the prepared nucleating agent POSS-DMDBS could decrease the spherulite size of iPP obviously, exhibiting higher nucleation density. The crystallization temperature was increased by 5 to 9°C when the content of POSS-DMDBS increased from 0.3 to 1 wt%. The non-isothermal crystallization kinetics showed that the crystallization rate of iPP/POSS-DMDBS increased with crystallization mechanism unvaried. The crystallization rate of iPP increased to the highest value when containing 1wt% POSS-DMDBS, even higher than that of iPP/DMDBS/POSS. Tensile modulus of iPP increased with the adding DMDB-POSS contents, while the elongation at break went down. The introduction of POSS-DMDBS in a small amount could improve the crystallization properties of iPP which would make sense for industrial applications.

REFERENCES

1. A. Fina, D. Tabuani, A. Frache, and G. Camino, *Polymer*, **46**, 7855 (2005).
2. E.L. Heeley, D.J. Hughes, P.G. Taylor, and A.R. Bassindale, *RSC Adv*., **5**, 34709 (2015).
3. F. Alves, P. Scholder, and I. Nischang, *ACS Appl. Mater. Interfaces*, **5**, 2517 (2013).
4. S. Roy, V. Scionti, S.C. Jana, C. Wesdemiotis, A.M. Pischera, and M.P. Espe, *Macromolecules*, **44**, 8064 (2011).
5. M. Dule, M. Biswas, T.K. Paira, and T.K. Mandal, *Polymer*, **77**, 32 (2015).
6. W. Zhang and A.H.E. Müller, *Prog. Polym. Sci*., **38**, 1121 (2013).
7. Z. Zhou, L. Cui, Y. Zhang, Y. Zhang, and N. Yin, *Eur. Polym. J*., **44**, 3057 (2008).
8. Z. Zhou, L. Cui, Y. Zhang, Y. Zhang, and N. Yin, *J. Polym. Sci*. Part B: *Polym. Phys*., **46**, 1762 (2008).
9. A. Durmus, A. Kasgoz, N. Ercan, D. Akın, and S. Şanlı, *Polymer*, **53**, 5347 (2012).
10. M. Schmidt, J.J. Wittmann, R. Kress, D. Schneider, S. Steuernagel, H.W. Schmidt, and J. Senker, *Cryst. Growth Des*., **12**, 2543 (2012).
11. B. Lotz, *Macromolecules*, **47**, 7612 (2014).
12. A. Menyhárd, M. Gahleitner, J. Varga, K. Bernreitner, P. Jääskeläinen, H. Øysæd, and B. Pukánszky, *Eur. Polym. J*., **45**, 3138 (2009).
13. K. Bernland, T. Tervoort, and P. Smith, *Polymer*, **50**, 2460 (2009).
14. Z. Horváth, B. Gyarmati, A. Menyhárd, P. Doshev, M. Gahleitner, J. Varga, and B. Pukánszky, *RSC Adv*., **4**, 19737 (2014).
15. B. Fillon, B. Lotz, A. Thierry, and J.C. Wittmann, *J. Polym. Sci*. Part B: *Polym. Phys*., **31**, 1395 (1993).
16. J. Lipp, M. Shuster, A.E. Terry, and Y. Cohen, *Langmuir*, **22**, 6398 (2006).
17. M. Takenaka, T. Kobayashi, T. Hashimoto, and M. Takahashi, *Phys. Rev. E*, **65**, 041401 (2002).
18. B.O. Okesola, V.n.M.P. Vieira, D.J. Cornwell, N.K. Whitelaw, and D.K. Smith, *Soft Matter*, **11**, 4768 (2015).
19. S. Roy, B.J. Lee, Z.M. Kakish, and S.C. Jana, *Macromolecules*, **45**, 2420 (2012).
20. S. Roy, J. Feng, V. Scionti, S.C. Jana, and C. Wesdemiotis, *Polymer*, **53**, 1711 (2012).
21. G. Chen, B. Feng, K. Zhu, Y. Zhao, and X. Yuan, *Chem. Res. Chin. Univ*., **31**, 303 (2015).
22. D.T.-v. Haeringen, J. Varga, G.W. Ehrenstein, and G.J. Vancso, *J. Polym. Sci*. Part B: *Polym. Phys*., **38**, 672 (2000).
23. C. Marco, G. Ellis, M.A. Gómez, and J.M. Arribas, *J. Therm. Anal. Calorim*., **68**, 61 (2002).
24. Y.F. Zhang, X. Li, and X.S. Wei, *J. Therm. Anal. Calorim*., **100**, 661 (2009).
25. A. Melvin, *J. Chem. Phys*., **12**, 1103 (1939).
26. J. Yu and J. He, *Polymer*, **41**, 891 (2000).
27. Y. Thomann, J. Suhm, R. Thomann, G. Bar, R.D. Maier, and R. Mulhaupt, *Macromolecules*, **31**, 5441 (1998).
28. M. Barczewski, M.D. Mizera, B. Dudziec, and T. Sterzynski, *J. Appl. Polym. Sci*., **131**, 40131 (2013).

DOI 10.1002/pen